

STRAIN-BASED FATIGUE FOR HIGH-STRENGTH ALUMINUM ALLOYS

N. E. Dowling¹, Attilio Arcari², C. A. Calhoun³, and D. C. Moore³

¹Professor, ²Graduate Research Assistant, ³Laboratory Assistant
Virginia Polytechnic Institute and State University, Blacksburg, Virginia, USA 24061
E-mail: ndowling@vt.edu

ABSTRACT

A study is reported of the cyclic deformation, fatigue, and mean stress relaxation behavior of extruded material of aluminum alloys 7075-T6511 and 7249-T76511. Experimental data and curve fitting constants are given for the cyclic stress-strain and strain-life curves. The stress-life (elastic strain) component of the strain-life curve shows a transition to a shallow slope at short life, necessitating a two-segment fit. Mean stress effects are included in the stress-life fit by applying the Walker mean stress method, and this is incorporated into the strain-life curve. Other mean stress relationships are also compared to the test data, specifically those of Goodman, Morrow, and Smith-Watson-Topper. Mean stress relaxation was observed even at quite low strain amplitudes where there is no measurable plastic deformation, with a transition in behavior to a strong relaxation effect at relatively large strains. Hence, the data are partitioned around $\epsilon_a = 0.006$ and different sets of relaxation constants using the Landgraf method are fitted above and below this level.

INTRODUCTION

Aluminum alloys 7075-T6511 and 7249-T76511 are being investigated to develop data and improved methodology for applying the strain-based approach in making fatigue life predictions for aircraft structural components. Of specific interest are the cyclic stress-strain and strain-life curves, characterization of mean stress effects, and modeling of mean stress relaxation. Aside from specific materials constants, the methodology presented is expected to be applicable to other high-strength aluminum alloys.

MATERIALS

Test material was obtained from extrusions of the two alloys. Properties from standard tensile tests parallel to the extrusion direction are given in Table 1. The 7075-T6511 and 7249-T76511 aluminum alloys studied are Al-Zn-Mg-Cu-Cr alloys that are members of the 7000-series of alloys, which are the highest strength class of aluminum alloys. Their strength arises from the combined effect of multiple precipitation hardening reactions involving the various alloying elements. Percentages of the alloying elements vary somewhat and are specified by the initial four digits, such as 7075. In processing, these alloys are first subjected to a solution heat treatment, followed by quenching. Then there is a second stage of heat treatment, called artificial aging, where the strengthening precipitates form at a moderately elevated temperature. For the 7075 alloy, the designation T6

indicates this process. Then the additional digits in T6511 indicate extruded material that has been stretched by about 2% after solution treatment, to relieve residual stresses, with some minor straightening after stretching also being permitted [1].

Alloy 7075 has been in wide use for more than 50 years in aircraft structural parts and other applications where high strength and light weight are critical. Alloy 7249 has been developed as a replacement for 7075 to achieve improved resistance to both exfoliation corrosion and stress corrosion cracking. Its aging treatment is carried beyond the point of peak strength, called overaging, as indicated by the T7 designation. The moderate degree of overaging is specified by the next digit as T76, and then the remaining digits in T76511 indicate extruded material with stress relief by stretching and minor straightening, as above. The overaging treatment for this special alloy may involve more than one stage of time and temperature to meet the strength and other property requirements of the specification AMS 4293 [2], with the exact details generally being proprietary to the extrusion supplier.

TEST SPECIMENS AND TEST METHODS

Unnotched, axially loaded test specimens were removed from the extrusion material with their long axes parallel to the extrusion direction. The specimens had a 15.24 mm (0.600 in) straight test section of diameter 7.62 mm (0.300 in). Strains were measured on the straight test section over a gage length of 12.7 mm (0.50 in). A gentle radius of 63.5 mm (2.5 in) was used to transition from the test section to the enlarged grip-end diameter. The test section and transition radius had only small amounts of

TABLE 1 – Tensile Properties

Aluminum Alloy	7075-T6511	7249-T76511
Elastic Modulus, E , MPa	70,336	70,004
Yield Strength, σ_o , MPa	561	567
Ultimate Strength, σ_u , MPa	611	601
Elongation, $100\epsilon_{pf}$, %	14.6	12.8
Reduction in Area, %	19.3	25.3
True Fracture Strength $\tilde{\sigma}_{fB}$, MPa	701	686
True Fracture Strain, $\tilde{\epsilon}_f$	0.214	0.292

material removed on each pass of final machining, and the final polishing was done in the longitudinal direction to a surface finish of approximately $0.1 \mu\text{m}$ ($4 \mu\text{in}$).

Approximately 50 specimens of each alloy were tested under cyclic loading using computer-controlled, closed-loop, servo-hydraulic test equipment. All tests involving considerable cyclic plasticity were conducted with controlled strain, as were some tests at nominally elastic levels, where the objective was to observe the relaxation of mean stress arising from biased strain limits. Other tests at nominally elastic levels were done with controlled stress (actually, force), some at zero mean stress, and others at non-zero mean stress.

Following the logic of Topper and coworkers [3, 4], initial overstrains (prestrains) were applied to most of the specimens prior to fatigue cycling. This consisted of 5 completely reversed, strain-controlled cycles at $\pm 1.2\%$ strain, followed by 10 additional cycles with peaks and valleys progressively decreasing to zero. This was done to advance the fatigue damage process, so that the behavior was similar to that during service loading with occasional severe cycles. Tests at strains higher than the prestrain level were not prestrained, as no effect is expected. For comparison purposes, a few zero-mean-stress tests at relatively low strains were done with no prestrain.

For each test, a stress-strain hysteresis loop recorded near half the fatigue life is employed to determine stable values of stress range $\Delta\sigma$, strain range $\Delta\epsilon$, and plastic strain range $\Delta\epsilon_p$, as illustrated in Fig. 1. For use in fitting the cyclic stress-strain and strain-life curves, these ranges are converted to amplitude quantities. For stress, strain, and plastic strain, respectively, the amplitudes are

$$\sigma_a = \Delta\sigma/2, \quad \epsilon_a = \Delta\epsilon/2, \quad \epsilon_{pa} = \Delta\epsilon_p/2 \quad (1)$$

If the hysteresis loop is not at least approximately symmetrical about zero stress, then the stable mean stress $\sigma_m = (\sigma_{\max} + \sigma_{\min})/2$ is also determined.

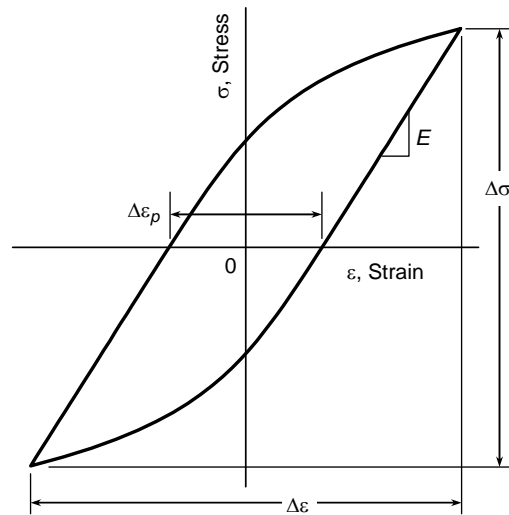


Figure 1 – Stress-strain hysteresis loop for stable behavior.

CYCLIC STRESS-STRAIN, STRAIN-LIFE, AND MEAN STRESS RELATIONSHIPS

Before presenting analysis of the test results, it is useful to describe the equations that are used to represent the cyclic stress-strain and strain-life curves, and also some equations for summarizing mean stress effects. In what follows, it is assumed that the test data involved are all obtained from axially loaded, unnotched test specimens.

Cyclic Stress-Strain Curve

To obtain the cyclic stress-strain curve, it is useful to note that σ_a/E is the elastic strain amplitude, where E is the elastic modulus. Further, the total strain amplitude ϵ_a is given by the sum of its elastic and plastic components.

$$\epsilon_a = \frac{\sigma_a}{E} + \epsilon_{pa} \quad (2)$$

Using values of stress amplitude σ_a and plastic strain amplitude ϵ_{pa} from stable stress-strain hysteresis loops, a power relationship fit is performed.

$$\sigma_a = H' \epsilon_{pa}^{n'} \quad (3)$$

where H' and n' are evaluated by least-squares regression.

Solving for the plastic strain amplitude in Eq. 3 and applying Eq. 2 then gives the desired relationship between the amplitudes of stress and total strain.

$$\epsilon_a = \frac{\sigma_a}{E} + \left(\frac{\sigma_a}{H'} \right)^{1/n'} \quad (4)$$

This is the familiar Ramberg-Osgood form.

Stress-Life and Strain-Life Curves

For fitting the strain-life curve, we employ values of stress amplitude σ_a and plastic strain amplitude ε_{pa} from stable stress-strain hysteresis loops, along with the corresponding cyclic fatigue life N_f for each test. Separate power relationships are fitted to stress versus life and to plastic strain versus life.

$$\sigma_a = \sigma'_f (2N_f)^b, \quad \varepsilon_{pa} = \varepsilon'_f (2N_f)^c \quad (\text{a, b}) \quad (5)$$

Applying Eq. 2 then gives

$$\varepsilon_a = \frac{\sigma'_f}{E} (2N_f)^b + \varepsilon'_f (2N_f)^c \quad (6)$$

Usually, only data for completely reversed (zero mean stress) tests are employed, and the fitting constants σ'_f , b , ε'_f , and c are considered to represent materials properties for the zero mean stress case. Equation 6 is commonly called the Coffin-Manson curve.

Mean Stress Relationships

A number of equations have been proposed and are in use for handling nonzero mean stresses. These can be expressed generically as functions

$$\sigma_{ar} = f(\sigma_a, \sigma_m) \quad (7)$$

which provide estimates of an *equivalent completely reversed stress amplitude* σ_{ar} , as calculated from the stress amplitude σ_a and mean stress σ_m that occur together for a situation of nonzero mean stress.

Noting that the stress-life relationship of Eq. 5(a) is obtained from tests at zero mean stress, it should be employed for our present purposes as

$$\sigma_{ar} = \sigma'_f (2N_f)^b \quad (8)$$

Hence, for a given situation of stress amplitude σ_a and mean stress σ_m , a value of $\sigma_{ar} = f(\sigma_a, \sigma_m)$ is calculated and then substituted into Eq. 8, which is solved for the life N_f as affected by the nonzero mean stress.

One of the most commonly used expressions for σ_{ar} is the Goodman relationship [5], as modified by J. O. Smith [6], which employs the ultimate tensile strength, σ_u .

$$\sigma_{ar} = \frac{\sigma_a}{1 - \frac{\sigma_m}{\sigma_u}} \quad (9)$$

The Morrow [7] equation has the same form, but in place of σ_u , employs the true fracture strength $\tilde{\sigma}_{fB}$, as corrected for hoop stress according to Bridgman [8]. A more commonly used alternate form similarly employs the constant σ'_f of Eq. 5(a) and 8, so that the two are

$$\sigma_{ar} = \frac{\sigma_a}{1 - \frac{\sigma_m}{\tilde{\sigma}_{fB}}}, \quad \sigma_{ar} = \frac{\sigma_a}{1 - \frac{\sigma_m}{\sigma'_f}} \quad (\text{a, b}) \quad (10)$$

The relationship of Smith, Watson, and Topper [9] does not employ a materials constant. Two equivalent forms, related by manipulations employing the definition of the stress ratio, $R = \sigma_{\min} / \sigma_{\max}$, are

$$\begin{aligned} \sigma_{ar} &= \sqrt{\sigma_{\max} \sigma_a} & (\text{a}) \\ \sigma_{ar} &= \sigma_{\max} \sqrt{\frac{1-R}{2}} & (\text{b}) \end{aligned} \quad (11)$$

Another approach is that of Walker [10], which is similar to the Smith-Watson-Topper (SWT) one, but includes a materials property γ . Two corresponding equivalent forms are

$$\begin{aligned} \sigma_{ar} &= \sigma_{\max}^{1-\gamma} \sigma_a^\gamma & (\text{a}) \\ \sigma_{ar} &= \sigma_{\max} \left(\frac{1-R}{2} \right)^\gamma & (\text{b}) \end{aligned} \quad (12)$$

Since $\sigma_{\max} = \sigma_m + \sigma_a$, and $\sigma_{\min} = \sigma_m - \sigma_a$, it is seen that Eqs. 11 and 12 do indeed provide relationships of the Eq. 7 type.

For the Walker equation, a single fitting procedure, that includes fatigue test data at zero and nonzero mean stresses, can be employed to obtain the constant γ along with σ'_f and b . This is done by combining Eqs. 8 and 12(b), solving for N_f , and then taking the logarithm of both sides of the resulting expression, which yields

$$\log(2N_f) = \frac{1}{b} \log \sigma_{\max} + \frac{\gamma}{b} \log \left(\frac{1-R}{2} \right) - \frac{1}{b} \log \sigma'_f \quad (13)$$

Then let

$$y = \log(2N_f), \quad x_1 = \log \sigma_{\max}, \quad x_2 = \log \left(\frac{1-R}{2} \right) \quad (14)$$

A multiple linear regression $y = m_1 x_1 + m_2 x_2 + d$ then provides values of the desired constants σ'_f , b , and γ .

Strain-Life Equations Including Mean Stress

Any of the mean stress relationships just described can be incorporated into the strain-life curve in a mathematically consistent manner [11]. To develop this methodology, first combine Eqs. 7 and 8 to obtain

$$\sigma_{ar} = \sigma_a \frac{f(\sigma_a, \sigma_m)}{\sigma_a} = \sigma'_f (2N_f)^b \quad (15)$$

Then solve for the stress amplitude σ_a in the numerator of the middle expression, and manipulate the result, to develop a form analogous to Eq. 5(a).

$$\sigma_a = \sigma'_f (2N^*)^b, \text{ where } N^* = N_f \left(\frac{\sigma_a}{f(\sigma_a, \sigma_m)} \right)^{1/b} \quad (a, b) \quad (16)$$

Hence, one can determine the life N^* from Eq. 16(a) that is expected for a given stress amplitude σ_a under zero mean stress, and then estimate the actual life N_f , as affected by a nonzero mean stress, by solving Eq. 16(b) for N_f .

$$N_f = N^* \left(\frac{\sigma_a}{f(\sigma_a, \sigma_m)} \right)^{-1/b} \quad (17)$$

The effect on life must be the same regardless of whether one employs a stress-life or a strain-life curve. This permits Eq. 6 to be generalized to

$$\varepsilon_a = \frac{\sigma'_f}{E} (2N^*)^b + \varepsilon'_f (2N^*)^c \quad (18)$$

Here, N^* is the life calculated from the strain amplitude ε_a as if the mean stress were zero, and then the actual life N_f , as adjusted for the effect of a nonzero mean stress, is obtained from Eq. 17. Equation 18 implies that a plot of strain amplitude versus N^* should correlate data at various mean stresses all onto this single strain-life curve.

In a paper by Dowling [12], the success of the mean stress relationships of Eqs. 9 to 12 were examined for a number of sets of test data on steels, aluminum alloys, and one titanium alloy. The Walker relationship, Eq. 12, was found to give superior results, and so it is considered to be of special interest here. In this case, Eq. 16(b) becomes

$$N_w^* = N_f \left(\frac{1-R}{2} \right)^{(1-\gamma)/b} \quad (19)$$

where a subscript w has been added to specify use of the Walker relationship.

DATA FITS FOR CYCLIC STRESS-STRAIN, STRESS-LIFE, AND STRAIN-LIFE CURVES

We will now proceed to present analysis of the test data obtained. There are separate subheadings treating the cyclic stress-strain, stress-life, and strain-life curves. For the life curves, the Walker mean stress equation is included in the data fitting. Then the next major section will consider comparisons of the test data with the other mean stress equations given above. This will be followed by a section on the modeling of mean stress relaxation, and then discussion and conclusions, combined in a section on concluding remarks.

Cyclic Stress-Strain Curve Fits

Cyclic stress-strain curves fitted to the test data for the 7075-T6511 and 7249-T76511 alloys are shown in Fig. 2. Equation 4 was found to represent the data very well, and the resulting constants are given in Table 2. Since very small values of plastic strain are difficult to measure accurately and may disturb the fitting of the larger, more accurately known values, data with $\varepsilon_{pa} < 0.00025$ were not employed in the Eq. 3 fit that was needed for Eq. 4.

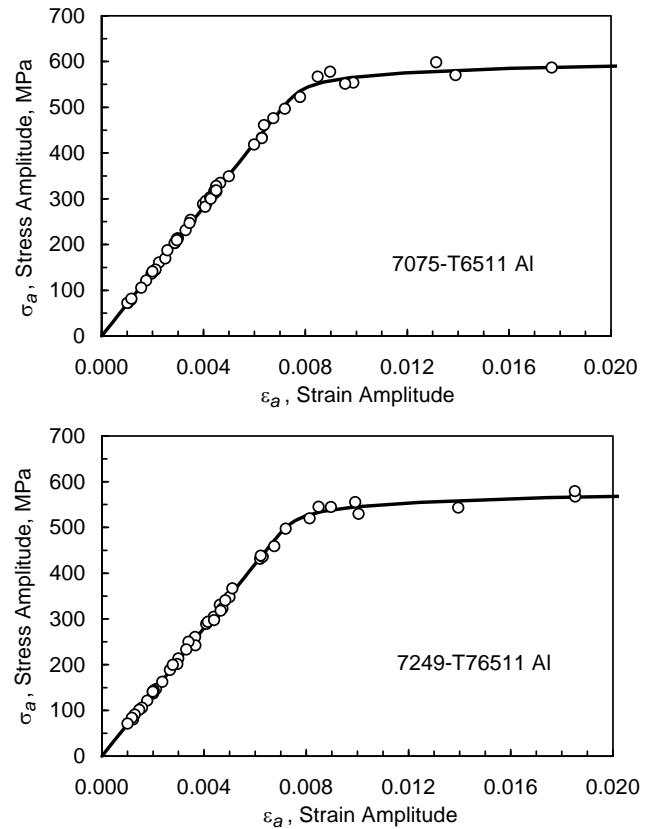


Figure 2 – Cyclic stress-strain curves for the two alloys.

TABLE 2 – Cyclic Stress-Strain and Strain-Life Constants

Aluminum Alloy	7075-T6511	7249-T76511
E , MPa	70,336	70,004
H' , MPa	655	633
n'	0.02335	0.02435
σ'_o (cyclic yield strength)	567	544
σ'_{fw} , MPa (Walker fit)	2780	3250
b_w (Walker fit)	-0.2010	-0.2187
γ (Walker fit)	0.4763	0.4933
σ'_{f2} , MPa (short life)	788	745
b_2 (short life)	-0.05164	-0.04759
N_i , cycles (intersection)	2318	2733
ϵ_{ai} (intersection)	0.00752	0.00742
ϵ'_{fw} , MPa	0.3465	0.3871
c_w	-0.8460	-0.8130

The 0.2% offset cyclic yield strengths on these curves are included in Table 2. These differ by only a small amount from the corresponding 0.2% offset yield strengths from tensile tests in Table 1. This indicates that these alloys have nearly stable behavior under cyclic loading, that is, they exhibit very little cycle dependent hardening or softening.

Stress-Life Curve Fits

Stress-life data and fitted lines are shown in Fig. 3 for the 7075 alloy. The corresponding graph for the 7249 alloy is not presented, but it is quite similar. For both alloys, there appear to be two distinct trends, with a shallow slope at short lives and a steeper slope at intermediate and long lives. Hence, separate stress-life fits were done for the two regions. A number of cycles $N_2 = 2000$ was chosen by judgment as the separation between the two regions, with this value applying to both alloys.

The fit employing Eqs. 13 and 14 was applied only to the data with $N_f > N_2$, which included all data with mean stresses that differed significantly from zero. The resulting equation is represented by

$$\sigma_{ar} = \sigma'_{fw}(2N_f)^{b_w} \quad (N_f \geq N_i) \quad (20)$$

used with Eq. 12. The subscript w is added to the fitting constants to indicate the fitting of data at various mean stresses using the Walker equation, in which fitting the value of γ is also obtained. Table 2 gives the resulting values of the three constants σ'_{fw} , b_w , and γ for both alloys.

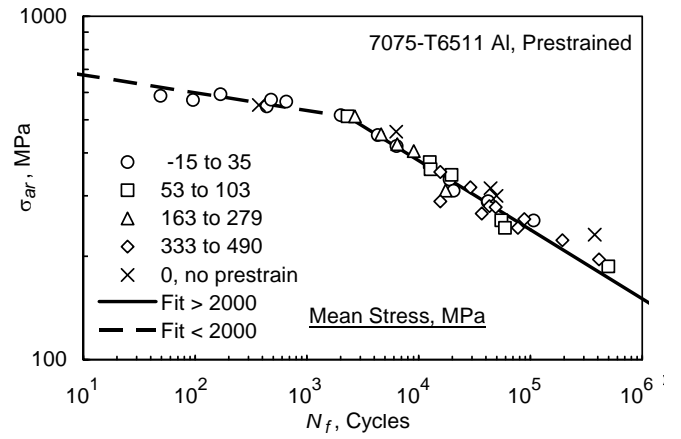


Figure 3 – Stress-life data and fit for the 7075 alloy based on the Walker mean stress equation at intermediate and long lives, with a separate fit employed at short lives.

The data for $N_f < N_2$ were then fitted separately, with the fitting constants being identified by adding a subscript 2.

$$\sigma_{ar} = \sigma'_{f2}(2N_f)^{b_2} \quad (N_f \leq N_i) \quad (21)$$

To employ such a two-segment fit, it is useful to determine the number of cycles N_i of the intersection point.

$$\log(2N_i) = \frac{\log(\sigma'_{fw}/\sigma'_{f2})}{b_2 - b_w}, \quad N_i = \frac{1}{2}10^{\log(2N_i)} \quad (22)$$

These expressions can be verified by equating the stress values of Eqs. 20 and 21 and solving for $N_f = N_i$. Values of N_i and the fitting constants for Eq. 21 are also given in Table 2 for both alloys.

Some data points are shown in Fig. 3 for tests with no prestrain. These are not included in the fitting and are seen to lie a little above the trend of the other data, indicating lives that are modestly longer than for prestrained samples.

Strain-Life Curve Fits

Now consider the strain-life curve as represented by Eq. 18, which by the use of $N^* = N_w^*$ is generalized to include nonzero mean stresses according to the Walker equation. From Eq. 16, the first term of Eq. 18 is seen to be equivalent to Eq. 20 or 21 used with Eq. 12(b), where the appropriate constants are employed, depending on whether the strain amplitude is greater or less than a value ϵ_{ai} that corresponds to N_i . In the high strain, short life region, $\epsilon_a \geq \epsilon_{ai}$, mean stresses relax close to zero, and so it is not useful or even feasible to try to determine a specific γ value for this region. Hence, the same γ value as determined from the Walker fit at intermediate and short lives is used.

The second term of Eq. 18 also needs to be fitted, requiring a relationship analogous to Eq. 5(b).

$$\varepsilon_{pa} = \varepsilon'_{fw} (2N_w^*)^{c_w} \quad (23)$$

Zero-mean-stress-equivalent life values N_w^* from Eq. 19 are thus fitted with plastic strain amplitudes. For Eq. 19, we use $b = b_w$ or b_2 depending on whether the N_f value for the particular test corresponding to ε_{pa} is longer or shorter, respectively, than N_i . The constants again have subscripts w added, to distinguish them from constants for Eq. 5(b) fitted merely to N_f values from zero-mean-stress tests.

For fitting Eq. 23, the same logic as before led to data not being included where $\varepsilon_{pa} < 0.00025$. Also, preliminary fitting gave a very high value of the intercept constant ε'_{fw} and did not seem to represent the shortest life data points very well. Hence, it was decided to include in the fit the true plastic strain corresponding to the fracture point in a tension test, taking this to correspond to a fatigue test with failure at $N_f = 0.5$ cycles. This true plastic fracture strain $\tilde{\varepsilon}_{pf}$ is obtained by applying Eq. 2 with values from Table 1.

$$\tilde{\varepsilon}_{pf} = \tilde{\varepsilon}_f - \frac{\tilde{\sigma}_{fB}}{E} \quad (24)$$

This procedure did indeed produce a more reasonable result, and the resulting fitting constants for Eq. 23 are listed in Table 2.

By assembling the results of the stress-life and plastic-strain-versus-life fits as described, we have all of the items needed for the complete strain-life curve. Due to the discontinuity in the stress-life behavior, there are two sets of equations.

$$\varepsilon_a = \frac{\sigma'_{fw}}{E} (2N_w^*)^{b_w} + \varepsilon'_{fw} (2N_w^*)^{c_w} \quad (25)$$

$$N_w^* = N_f \left(\frac{1-R}{2} \right)^{(1-\gamma)/b_w} \quad (\varepsilon_a \leq \varepsilon_{ai})$$

and

$$\varepsilon_a = \frac{\sigma'_{f2}}{E} (2N_w^*)^{b_2} + \varepsilon'_{fw} (2N_w^*)^{c_w} \quad (26)$$

$$N_w^* = N_f \left(\frac{1-R}{2} \right)^{(1-\gamma)/b_2} \quad (\varepsilon_a \geq \varepsilon_{ai})$$

Equation 25 applies at intermediate and long lives, specifically, for strain amplitudes $\varepsilon_a \leq \varepsilon_{ai}$. Note that ε_{ai} can be calculated by substituting $N_w^* = N_i$ and calculating the

strain amplitude. Then Eq. 26 applies at short lives, where $\varepsilon_a \geq \varepsilon_{ai}$, with the two curves joining at the discontinuity point (N_i, ε_{ai}) .

Curves corresponding to the combination of Eqs. 25 and 26 are shown in Fig. 4 along with all of the test data at all mean stresses for each alloy. There is only small scatter of the data about the discontinuous curves, indicating success of the manner of handling mean stress effects and the other aspects of the fitting procedure. Also shown in Fig. 4 are data points for tests with no prestrain, which were not included in the fitting. These are seen to lie a little above the trend of the other data.

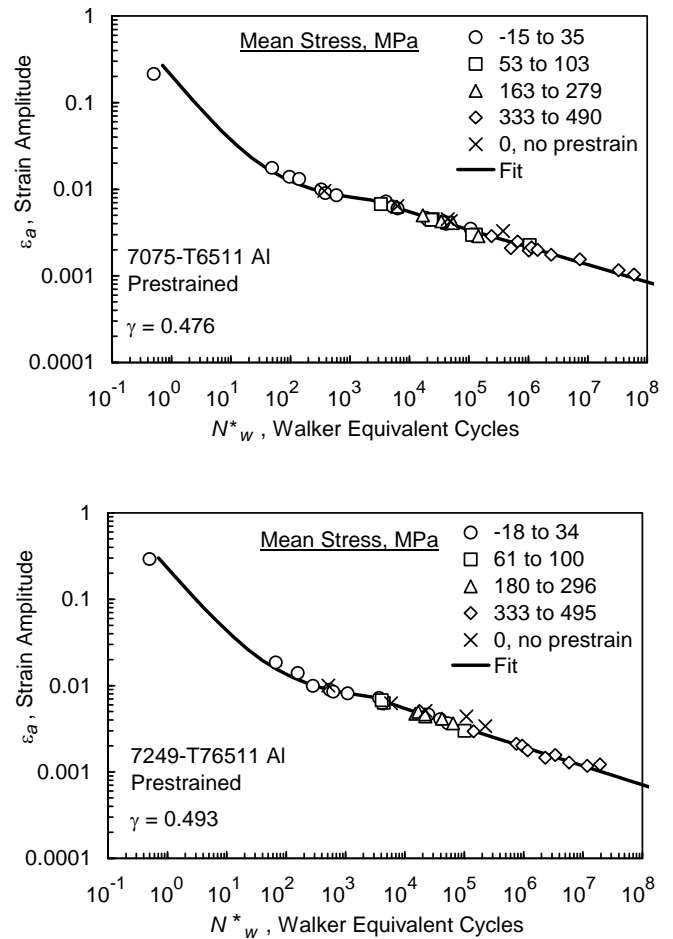


Figure 4 – Strain amplitude versus Walker equivalent life for the two alloys.

COMPARISON OF TEST DATA AND MEAN STRESS EQUATIONS

Two methods of comparison will be discussed under separate subheadings below: stress-life plots, and amplitude-mean plots. Then there will be a third subsection which adds some useful discussion.

Stress-Life Comparisons

The most direct way to compare test data to one of Eqs. 9 to 12 is as follows: Calculate σ_{ar} from the stresses applied in each test and plot the resulting values versus the corresponding experimental fatigue lives. Such comparisons are shown for the 7075 alloy in Figs. 5 to 8 for the mean stress relationships of Eqs. 9, 10(a), 10(b), and 11, respectively. On each of these graphs, a line of the Eq. 5(a) form is also shown, which represents a fit to the data with zero mean stress. Only data in the range 10^3 to 10^6 cycles are shown, as data at shorter lives involved only small mean stresses. Corresponding graphs for the 7249 alloy show quite similar trends.

The extent to which the data on such a plot agree with the zero-mean-stress line is a measure of the success of the σ_{ar} equation used. For the Goodman relationship, Eq. 9, which employs the ultimate tensile strength, it is clear from Fig. 5 that the correlation is quite poor. Data for tensile mean stresses lie well above the zero mean line, indicating

that actual lives are often much longer than estimated, that is, the method is excessively conservative with respect to life estimates.

From Fig. 6, the Morrow relationship of Eq. 10(a), employing the true fracture strength $\tilde{\sigma}_{fB}$, gives better results. However, from Fig. 7, we see that Eq. 10(b), which uses the fitting constant σ'_f , performs very poorly and is grossly nonconservative with respect to life estimates. In Fig. 8, the SWT relationship of Eq. 11 gives quite good results, with the correlation being better than for the Goodman relationship or either form of the Morrow equation.

An analogous correlation plot for the Walker relationship, Eq. 12, has already been shown as Fig. 3, where the $N_f \geq N_i$ portion is of primary interest here. In this case, the comparison is made to the Eq. 20 fit of data at various mean stresses, where the value of γ from this fit is employed with Eq. 12. The correlation is similar to that for the SWT method, but slightly better, as might be expected from the ability to vary γ to obtain an optimum fit.

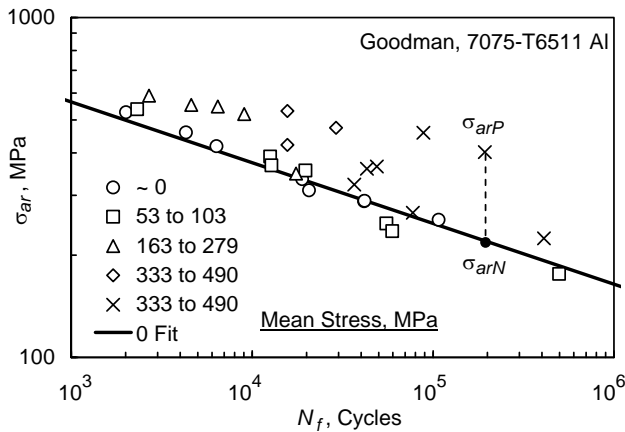


Figure 5 – Equivalent completely reversed stress amplitude versus life correlation for the 7075 alloy for the Goodman equation.

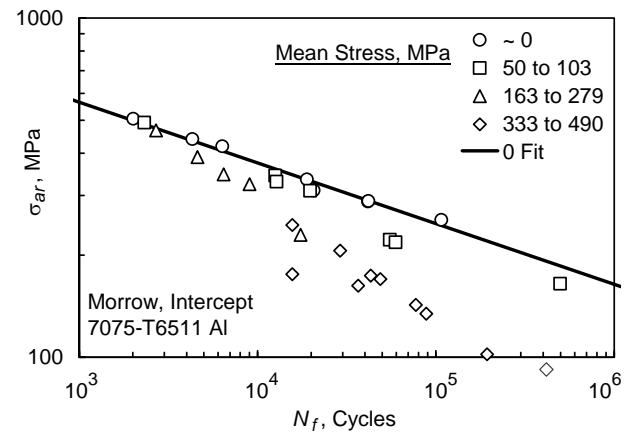


Figure 7 – Equivalent completely reversed stress amplitude versus life correlation for the 7075 alloy for the Morrow intercept equation.

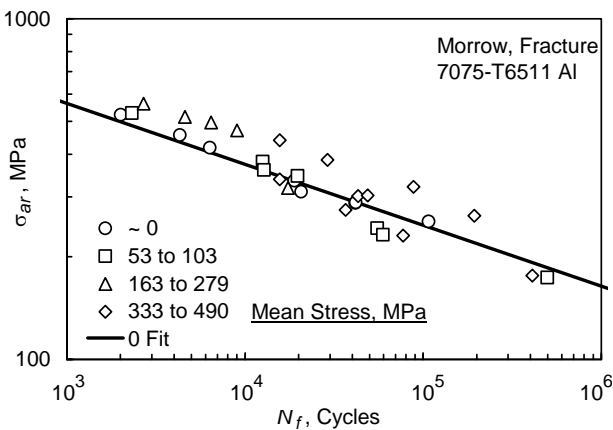


Figure 6 – Equivalent completely reversed stress amplitude versus life correlation for the 7075 alloy for the Morrow fracture strength equation.

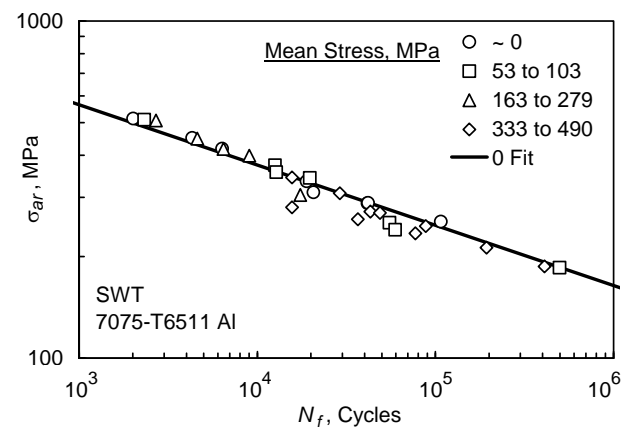


Figure 8 – Equivalent completely reversed stress amplitude versus life correlation for the 7075 alloy for the Smith-Watson-Topper equation.

Amplitude-Mean Plots

Another means of comparing mean stress equations to test data is to employ amplitude-mean plots, as shown for both alloys in Figs. 9 and 10. For these, it is necessary to calculate σ_{ar} for each test data point from the experimental fatigue life N_f , using the stress-life relationship for zero mean stress. Equation 5(a) with appropriate constants is employed, except for the Walker equation, where Eq. 20 applies.

For the Goodman and Morrow relationships, Eqs. 9, and 10, straight lines are expected on a plot of the normalized stress amplitude σ_a / σ_{ar} versus mean stress σ_m . These are seen in Fig. 9 for the two alloys. The Goodman equation gives a line that intercepts the mean stress axis at the ultimate tensile strength σ_u . The experimental data points are seen to lie beyond this line. Hence, as for the life plots, for tensile mean stresses, this method is seen to be overly conservative with respect to life estimates. The Morrow equation with intercept $\tilde{\sigma}_{fB}$ gives good agreement, but the form using the intercept σ'_f gives grossly a nonconservative comparison. This latter trend seems to be associated with the transition in stress-life behavior seen in Fig. 3, as the intercept σ'_f fitted in the intermediate and long life region is

a very high value that is far above the intercept for the short-life region, which is more similar to the true fracture strength.

Equations 11 and 12 form a family of curves on plots similar to Fig. 9, so a comparison of this type is not very useful. But a single curve is formed on a plot of σ_a / σ_{ar} versus σ_m / σ_{ar} , as seen in Fig. 10. Note that the SWT relationship, Eq. 11, corresponds to the $\gamma = 0.5$ special case of the Walker relationship, Eq. 12. Since the fitted γ values for the Walker equation were both near 0.5, the two curves for each alloy are quite close, and it is difficult to decide from these plots which provides better agreement with the test data.

Discussion

A numerical quantity that characterizes the degree of correlation on a life plot such as Figs. 5 to 8 can be determined as follows: Consider the points σ_{arP} and σ_{arN} in Fig. 5. The former point corresponds to the applied stresses and experimental life for a fatigue test, and the latter to the point on the zero-mean-stress fit at the same life. The difference $\sigma_{arP} - \sigma_{arN}$ is a measure of the lack of correlation, and a dimensionless measure is obtained by normalized this difference to the σ_{arN} value.

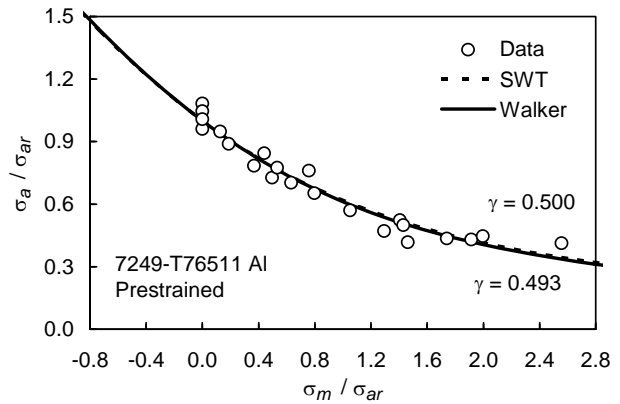
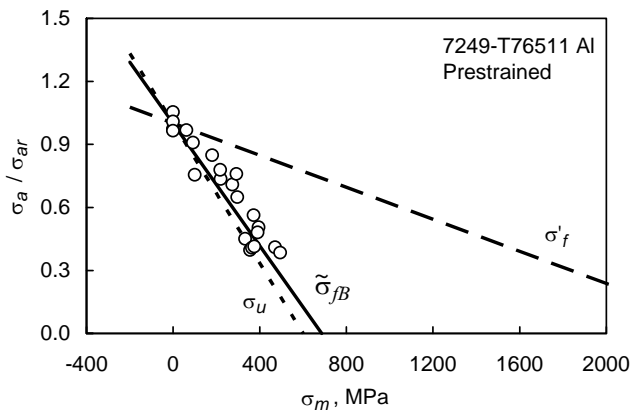
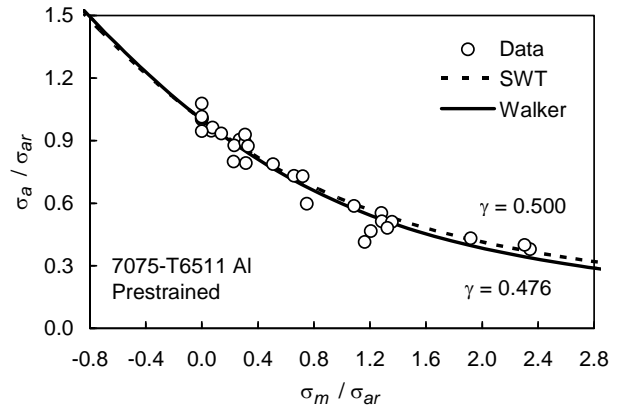
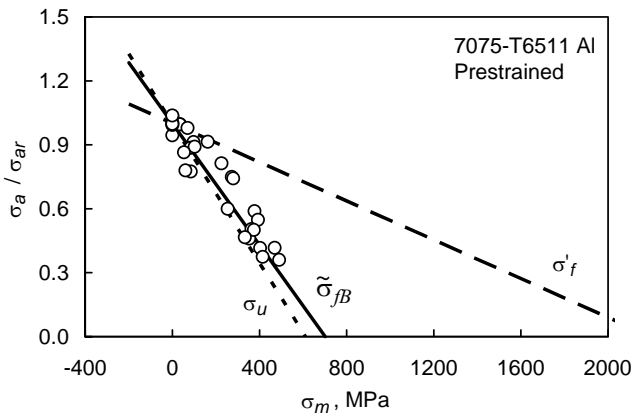


Figure 9 – Normalized stress amplitude-mean plots for the two alloys.

Figure 10 – SWT and Walker amplitude-mean plots for the two alloys.

$$z = \frac{\sigma_{arP} - \sigma_{arN}}{\sigma_{arN}} = \frac{\sigma_{arP}}{\sigma_{arN}} - 1 \quad (27)$$

A measure of the overall scatter for a set of data is the standard deviation of the variable z . Considering all nonzero mean stress data points in a given comparison, where n is the number of these, we have

$$s_z = \sqrt{\frac{\sum_{i=1}^n z_i^2}{n-1}} \quad (28)$$

We will term this s_z the *stress deviation*. To similarly summarize the success of a Walker equation fit, such as the $N_f \geq N_i$ portion of Fig. 3, the same equations apply. But since all of the data points are employed in the Eq. 20 fit, including the zero mean stress ones, even these are included in the calculation of s_z .

Values of s_z for each of the mean stress equations are given in Table 3. The trends noted above are also seen in these values. The Goodman and Morrow σ'_f equations give relatively large values of s_z , indicating highly inaccurate results, whereas the Morrow $\tilde{\sigma}_{fB}$ equation is considerably better, and the SWT equation is better yet. The Walker equation gives a slightly lower s_z than the SWT one, and so it is the most accurate of the mean stress equations studied. Hence, its use in representing the strain-life curve is justified.

TABLE 3 – Values of Stress Deviations for Mean Stress Equations

Mean Stress Equation	Values of s_z	
	7075-T6511	7249-T76511
Goodman	0.352	0.442
Morrow, $\tilde{\sigma}_{fB}$	0.157	0.194
Morrow, σ'_f	0.324	0.370
Smith-Watson-Topper	0.074	0.068
Walker, fitted γ	0.057	0.055

An extensive study where the same mean stress equations were applied to a number of sets of data is described by Dowling [12]. Similar trends in the success of the various equations occurred for the 9 sets of aluminum alloy data that were included. Values of γ were around 0.5 for all of the relatively high strength aluminum alloys, which included 2014, 2024, and 7075 alloys. But for relatively low strength alloys, such as 6061, the value of γ was around 0.65. Also, for three sets of data on 2024 and 6061 alloys, where short fatigue lives were included from strain-controlled tests, similar flattening of the stress-life curve at short lives occurred.

MODELING OF MEAN STRESS RELAXATION

Strain controlled tests with a nonzero mean strain produce an initial mean stress that tends to relax toward zero. Depending on the strain amplitude, the mean stress may relax very little, or by a moderate amount that stabilizes short of zero, or completely to approximately zero. Less relaxation occurs if the strain amplitude is small and mostly elastic, and more relaxation occurs for larger strain amplitudes that include a larger plastic strain component. Some test data illustrating this effect are shown in Figs. 11 and 12 for the 7075 and 7249 alloys under study here.

A study of this behavior and its modeling is reported by Arcari [13], with the results being briefly summarized here. The empirical relaxation model of Landgraf [14] was found to provide acceptable results. Here, the mean stress relaxation is modeled as a power equation with the number of cycle as base.

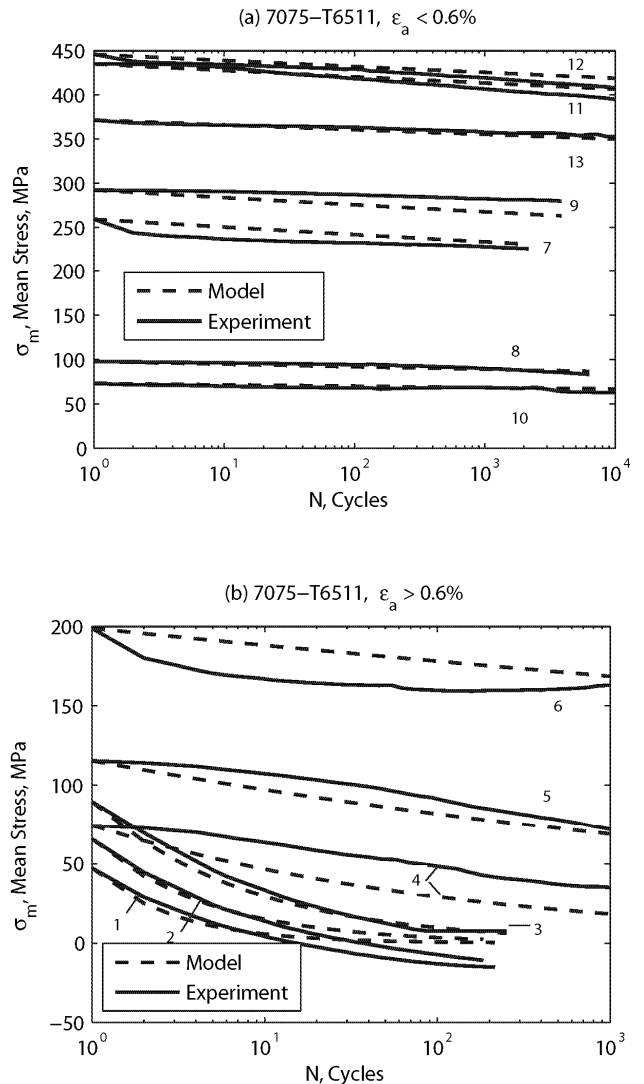


Figure 11 – Mean stress relaxation in the 7075 alloy for (a) low strain amplitudes and (b) high strain amplitudes.

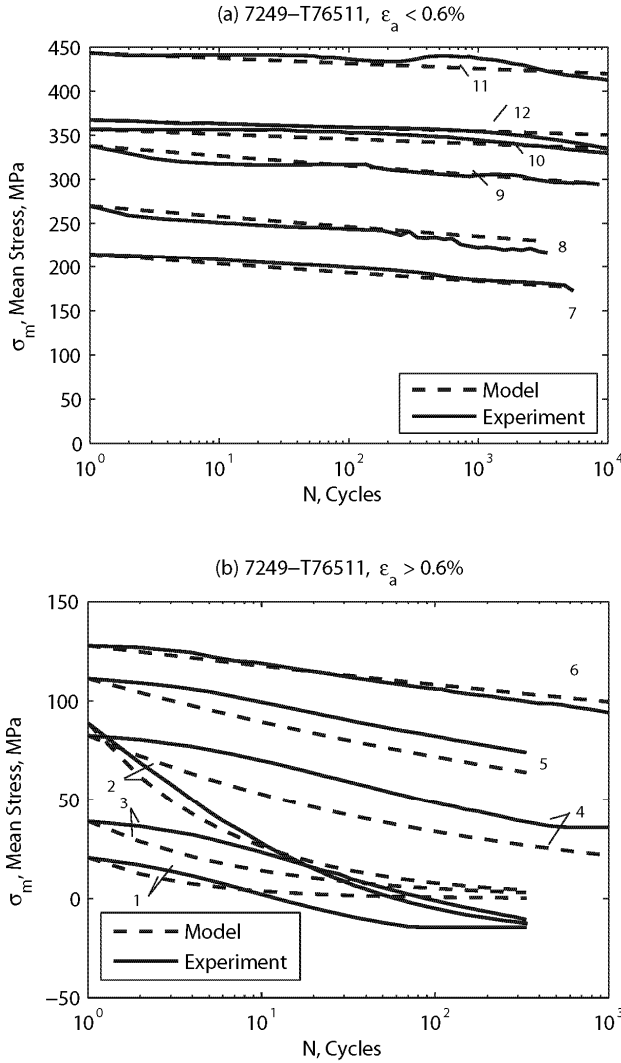


Figure 12 – Mean stress relaxation in the 7249 alloy for (a) low strain amplitudes and (b) high strain amplitudes.

$$\sigma_{mN} = \sigma_{mi} N^r \quad (a)$$

$$\text{where } r = A \left(1 - \frac{\varepsilon_a}{\varepsilon_{aTh}} \right) \quad (b) \quad (29)$$

In these equations, σ_m is mean stress, with an additional subscript i indicating the initial value, and an additional subscript N the value after N cycles. The quantity r is a relaxation exponent that varies linearly with strain amplitude, ε_a , and which has a negative value. Also, ε_{aTh} is a threshold value of strain amplitude, below which there is no relaxation, and A is an additional fitting constant.

However, the results were somewhat surprising in that relaxation was observed even at quite low strain amplitudes where there is no measurable plastic deformation. Further, there was a fairly distinct transition in behavior between this behavior at low strain amplitudes and the strong relaxation effect that occurs at relatively large strains. To apply Eq. 29,

it was necessary to partition the data around $\varepsilon_a = 0.006$ and to apply separate sets of constants ε_{aTh} and A in two different regions.

$$r = A_1 \left(1 - \frac{\varepsilon_a}{\varepsilon_{aTh1}} \right) \quad (\varepsilon_a \leq \varepsilon_{a12}) \quad (a)$$

$$r = A_2 \left(1 - \frac{\varepsilon_a}{\varepsilon_{aTh2}} \right) \quad (\varepsilon_a \geq \varepsilon_{a12}) \quad (b) \quad (30)$$

The resulting dependence of r on strain amplitude is shown in Fig. 13 for the 7249 alloy, with 7075 having quite similar behavior.

The plotted points shown in Fig. 13 correspond to Eq. 29(a) fitted to the mean stress versus cycles data for individual tests. However, each line is derived from a multiple regression applied to the variations of both strain amplitude and cycles for several tests. For each alloy, one such multiple regression was performed for all tests with $\varepsilon_a < 0.006$, and another for all tests with $\varepsilon_a > 0.006$. The strain amplitude where the two r versus ε_a lines from the separate fits intersect is denoted ε_{a12} .

Each multiple regression was performed by combining Eqs. 29(a) and (b), isolating the quantity $\sigma_{mN} / \sigma_{mi}$, and then taking the logarithm of both sides of the resulting expression.

$$\frac{\sigma_{mN}}{\sigma_{mi}} = N^{A(1-\varepsilon_a/\varepsilon_{aTh})}$$

$$\log \left(\frac{\sigma_{mN}}{\sigma_{mi}} \right) = A \log N - \frac{A}{\varepsilon_{aTh}} \varepsilon_a \log N \quad (31)$$

Then we let

$$y = \log \left(\frac{\sigma_{mN}}{\sigma_{mi}} \right) \quad (32)$$

$$x_1 = \log N, \quad x_2 = \varepsilon_a \log N, \quad b = 0$$

A multiple linear regression $y = m_1 x_1 + m_2 x_2 + b$ finally provides values of the fitting constants A and ε_{aTh} .

The resulting values of A and ε_{aTh} and their ranges of applicability (as separated by ε_{a12}) are given in Table 4 for the two alloys. Also, Figs. 11 and 12 show the curves from this modeling along with the test data. The modeling is in reasonable agreement with the overall trends of the data. For some of the tests at the highest strain amplitudes, the initially tensile mean stresses cross zero and tend to stabilize at a small compressive value, reflecting an asymmetry in the behavior of the material. However, the modeling equations require relaxation toward and not crossing zero.

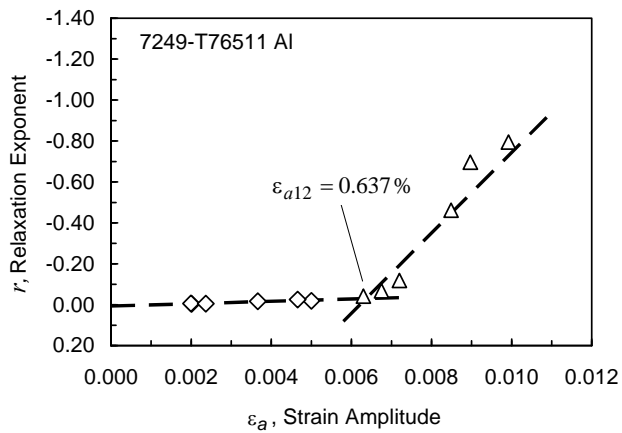


Figure 13– Relaxation exponent versus strain amplitude for the 7249 alloy.

Further work is ongoing on mean stress relaxation, including adding the small compressive bias to the behavior, as well as modeling of relaxation under variable amplitude loading.

CONCLUDING REMARKS

For aluminum alloys 7075-T6511 and 7249-T76511, we have presented cyclic stress-strain and strain-life curves and fitting constants. The former follows the Ramberg-Osgood form very well. The value of the strain hardening exponent n' is quite small, reflecting a flat cyclic stress-strain curve beyond the elastic region. Comparison of the yield strengths from tension tests and the cyclic stress-strain curves indicates that these alloys exhibit very little cycle dependent hardening or softening.

The strain-life curves conform to the Coffin-Manson form, except that the stress-life (elastic strain) component of the curve shows a transition in behavior to a shallow slope at short lives, necessitating a two-segment fit. This in turn results in a slope discontinuity in the strain-life curve. In the stress-life fit, data at various mean stresses were fitted all together using the Walker mean stress equation, which correlated the data very well. As a result, the strain-life fits include the effect of mean stress by incorporating the stress ratio $R = \sigma_{\min} / \sigma_{\max}$ and a Walker constant γ .

Other mean stress methods were also compared with the test data. The traditional Goodman equation gives very poor results, as does the Morrow equation in the form employing the stress-life fitting constant σ'_f . The former is overly conservative, and the latter dangerously nonconservative. The Morrow equation with the true fracture strength is reasonably accurate, and the Smith-Watson-Topper relationship is even better. The Walker equation gives superior results, but only modestly better than SWT, as the constant γ for both alloys was not very different than 0.5, which corresponds to the SWT method.

Mean stress relaxation was successfully modeled with the approach of Landgraf. Relaxation was observed even at

TABLE 4 – Mean Stress Relaxation Constants for the Landgraf Model

Alloy	Range	A	$\epsilon_a Th$
7075-T6511	$\epsilon_a \leq 0.648 \%$	-0.0006948	-0.0002374
	$\epsilon_a \geq 0.648 \%$	1.6350	0.006407
7249-T76511	$\epsilon_a \leq 0.637 \%$	0.006347	0.001095
	$\epsilon_a \geq 0.637 \%$	1.2196	0.006216

quite low strain amplitudes where there is no measurable plastic deformation, with a fairly distinct transition to the strong relaxation effect that occurs at relatively large strains. It was necessary to partition the data around $\epsilon_a = 0.006$ and to apply different sets of relaxation constants above and below this level.

The cyclic stress-strain curve fit for the 7249 alloy is reported as Fig. 14. The strain value ϵ_{ai} corresponding to the slope discontinuity in the strain-life curve is shown, as is the value ϵ_{a12} for the transition in mean stress relaxation behavior. The former is somewhat higher than the latter, but both occur near the end of the linear region of the curve, below the cyclic yield strength as defined by a 0.2% plastic strain offset. Very similar trends occur for the 7075 alloy but are not illustrated.

From the test data obtained, it is a noteworthy that the two aluminum alloys seem to behave in a very similar manner, both qualitatively and quantitatively.

As of this writing, testing continues on the two alloys. Included are fatigue life and mean stress relaxation tests involving compressive mean stresses. Hence, values of the various materials constants in Tables 2 to 4 will be refined later when additional test data are included. However, the test data obtained so far are quite extensive and are sufficient to justify employing the cyclic stress-strain, strain-life, and mean stress relaxation constants that are presented.

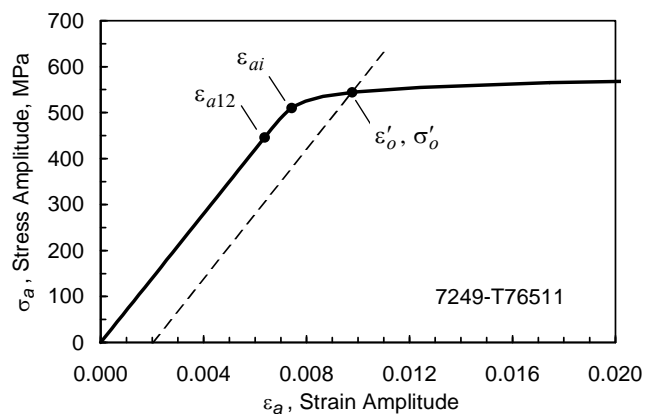


Figure 14 – Cyclic stress-strain curve for the 7249 alloy showing the strain-life transition ϵ_{ai} , the relaxation transition ϵ_{a12} , and the 0.2% offset cyclic yield strength.

ACKNOWLEDGEMENTS

This work was supported by the U. S. Naval Air Systems Command, Patuxent River, MD. Technical direction was provided by Nam D. Phan of NAVAIR Structures, with the aid of Trung T. Nguyen. Nagaraja Iyyer of Technical Data Analysis, Inc., Falls Church, VA, was helpful in a variety of ways. Project administration was handled by Pamela F. Bowen of Integrated Systems Solutions, Inc., California, MD. Gratitude is expressed to these individuals and organizations for their able assistance.

Institutional support was provided by the Engineering Science and Mechanics Department, and by the Materials Science and Engineering Department, Virginia Tech, Blacksburg, VA.

REFERENCES

- [1] Davis, J. R., ed., *Metals Handbook: Desk Edition, 2nd ed.*, ASM International, Materials Park, OH, 1998.
- [2] SAE International, "Aluminum Alloy Extrusions, 7.9Zn-1.6Cu-2.2Mg-0.16Cr (7249-T76511), Solution Heat Treated, Stress-Relieved, Straightened, and Overaged," Aerospace Material Specification, AMS 4293, SAE International, Warrendale, PA, 2008.
- [3] Topper, T. H., and Sandor, B. I., "Effects of Mean Stress and Prestrain on Fatigue Damage Summation," *Effects of Environment and Complex Load History on Fatigue Life, ASTM STP 462*, Am. Soc. for Testing and Materials, Philadelphia, PA, 1970, pp. 93-104.
- [4] Watson, P., and Topper, T. H., "The Effects of Overstrains on the Fatigue Behavior of Five Steels," *1970 Fall Meeting of the Metallurgical Society of AIME*, Cleveland, OH, Oct. 1970. See also: Watson, P., *The Effect of Mean Stress and Overstrains on the Fatigue Behavior of Structural Steels*, PhD Dissertation, Department of Civil Engineering, University of Waterloo, Ontario, Canada, 1971.
- [5] Goodman, J., *Mechanics Applied to Engineering*, Longmans, Green and Co., London, 1919, pp. 631-636.
- [6] Smith, J. O., *The Effect of Range of Stress on the Fatigue Strength of Metals, Bulletin No. 334*, University of Illinois, Engineering Experiment Station, Urbana, IL, Feb. 1942. See also *Bulletin No. 316*, Sept. 1939.
- [7] Morrow, J., "Fatigue Properties of Metals, Section 3.2," *Fatigue Design Handbook, Pub. No. AE-4*, Soc. of Automotive Engineers, Warrendale, PA, 1968. Section 3.2 is a summary of a paper presented at Division 4 of the SAE Iron and Steel Technical Committee, Nov. 4, 1964.
- [8] Bridgman, P. W., "The Stress Distribution at the Neck of a Tension Specimen," *Trans. of the Am. Soc. for Metals*, Vol. 32, 1944, pp. 553-574.
- [9] Smith, K. N., Watson, P., and Topper, T. H., "A Stress-Strain Function for the Fatigue of Metals," *Jnl. of Materials, ASTM*, Vol. 5, No. 4, 1970, pp. 767-778.
- [10] Walker, K., "The Effect of Stress Ratio During Crack Propagation and Fatigue for 2024-T3 and 7075-T6 Aluminum," *Effects of Environment and Complex Load History on Fatigue Life, ASTM STP 462*, Am. Soc. for Testing and Materials, Philadelphia, PA, 1970, pp. 1-14.
- [11] Dowling, N. E., "Mean Stress Effects in Stress-Life and Strain-Life Fatigue," *Fatigue 2004: Second SAE Brazil International Conference on Fatigue*, São Paulo, Brazil, June 2004. See also: *SAE Paper No. 2004-01-2227*, SAE International, Warrendale, PA, 2004.
- [12] Dowling, N. E., Calhoun, C. A., and Arcari, A., "Mean Stress Effects in Stress-Life Fatigue and the Walker Equation," *Fatigue and Fracture of Engineering Materials and Structures*, Vol. 32, No. 3, March 2009.
- [13] Arcari, A., De Vita, R., and Dowling, N. E., "Mean Stress Relaxation During Cyclic Straining of High Strength Aluminum Alloys," Paper presented at the *Int. Conf. on Fatigue Damage of Structural Materials VII*, Sept. 14-19, 2008, Hyannis, MA. Accepted by the *International Journal of Fatigue*, 2009.
- [14] Landgraf, R. W., and Chernenkoff, R. A., "Residual Stress Effects on Fatigue of Surface Processed Steels," Champoux, R. L., et al., eds., *Analytical and Experimental Methods for Residual Stress Effects in Fatigue, ASTM STP 1004*, Am. Soc. for Testing and Materials, Philadelphia, PA, 1988, pp. 1-12.